Nonlinear Dyn
https://doi.org/10.1007/s11071-023-08547-y

ORIGINAL PAPER

A confidence ellipse analysis for stochastic dynamics model of Alzheimer's disease

Jianzhong Gao · Juping Ji · Yanping Liu · Feng Zhang · Ruiwu Wang · Hao Wang

Received: 27 October 2022 / Accepted: 16 March 2023

Abstract The Alzheimer's disease (AD) is a neurodegenerative disease, which is caused by the aggregation of beta-amyloid peptide ($A\beta$) in the patient's brain and the disorder of Ca^{2+} homeostasis in neurons. Caluwé and Dupont (Theor Biol 331:12–18, 2013) proposed a deterministic AD model to explore the effect of Ca^{2+} on AD. They demonstrated the positive feedback loop between $A\beta$ and Ca^{2+} : and the occurrence of bistability. Based on their results, we further discuss the bistable behaviors. We present two periodically feasible drug strategies to alleviate the AD and screen out more effective one. In this paper, we also formulate a stochastic AD model, analyze the existence and uniqueness of global positive solutions and establish sufficient conditions for the existence of ergodic stationary distribution. Furthermore, the confidence ellipses describing the configurational arrangement of stochastic coexistence equilibria are constructed by stochastic sensitivity function technique, and tipping threshold is estimated as well. Noise-induced stochastic switching between two coexistence equilibria is observed in bistability region. Our results provide a new idea to control noise to alleviate AD through physical therapy.

Keywords Bistability · Positive feedback loop · Environmental noise · Ergodic stationary · Confidence ellipse

1 Introduction

Alzheimer's disease (AD) is recognized as the leading disease in the elderly, usually causing irreversible brain dysfunction in humans [1, 2], while less than 10% of AD cases are familial and occur in people around the age of 30–50[3]. AD is divided into seven stages (Global Deterioration Scale): from normal cognition but pathological changes in the brain (stage 1) to poor mobility, communication difficulty, and the need for feeding assistance (stage 7) [4]. Importantly, cognitive dysfunction is major. Patients also often suffer from neuropsychiatric dysfunction, such as depression, anxiety, psychosis and circadian rhythm disorder [5]. Unfortunately, death occurs 3–10 years

J. Gao · R. Wang
School of Ecology and Environment, Northwestern Polytechnical University, Xi'an 710129, China

J. Ji · H. Wang (✉)
Department of Mathematical and Statistical Sciences, University of Alberta, Edmonton, AB T6G 2G1, Canada
e-mail: hao8@ualberta.ca

Y. Liu
School of Mathematics and Computer Application, Shangluo University, Shangluo 726000, China

F. Zhang (✉)
School of Statistics and Mathematics, Yunnan University of Finance and Economics, Kunming 650221, China
e-mail: fzhang188@163.com

Published online: 20 May 2023

after the onset of AD and is the result of inactivity, often leading to pneumonia and blood clots [6]. It was estimated that the incidence of AD doubles every five years after the age of 65, affecting 1275 per 100,000 people. The cases after 86 years old accounted for the 30–50% of total AD cases [7]. Countries around the world invest a large amount of money to mitigate the development of AD every year. According to statistics, the investment in 2015 was $ 818 billion, which was increased by 35.4% over 2010, and accounted for 1.09% of global GDP [8, 9], which greatly increases the economic burden of the country, and has a detrimental influence on human life, social harmony and stability. Currently, the cholinesterase inhibitors on the market for the treatment of AD include galantamine, donepezil, rivastigmine, memantine and herbal medicine. These drugs have long been considered the first line of treatment for AD. Unfortunately, reports have shown that although patients taking these drugs can alleviate the development of AD to some extent, these drugs can also produce certain side effects, such as diarrhea, nausea and vomiting. Few patients also experience life-threatening adverse effects such as thrombocytopenia, heart attack, adenocarcinoma and extreme anaemia. In addition, various different and contradictory assumptions have made it difficult to determine the exact mechanism and physiological function of the disease itself, as well as the obstacles of drug transport across the impenetrable blood–brain barrier [10]. Additionally, due to the inability to target the large area of neuron [11] and synaptic death in AD brain, the current treatment has also reached a bottleneck. However, some researchers have tried to break the shackles of the current treatment of AD by studying the mathematical modeling of AD [12–15]. For example, Helal et al. suggested that the polymerization rate of β-amyloid ($A\beta$) peptide is constant and also when it is described by a power law, and they proved the well-posedness and stability of model [15]. Oligomers are more toxic in the process of $A\beta$ aggregation, the elastic analysis showed that $A\beta_{42}$ paranuclei can be used as therapeutic target [12]. Dayeh et al. proposed $A\beta$ mathematical model for monomer aggregation into oligomers by the concepts of chemical dynamics and population dynamics. They investigated the stable and unstable conditions of equilibrium, and also gave the formula of the amount of monomers needed for the production of oligomer [13]. Although the research on AD has been carried out and achieved substantial results, the potential mechanism of AD is still unclear. Therefore, it is urgent to explore the potential molecular mechanisms leading to AD.

The pathogenesis of AD is accompanied by highly complex ecological processes. It is widely believed that the beta-amyloid ($A\beta$) lesion, cholinergic and tau hypothesis are three primary inducements of AD [3]. At present, a reasonable explanation for causing AD is the aggregation of β-amyloid peptide ($A\beta$) in the brain of patients. Pathologically, a large number of plaques (composed of $A\beta$-peptide) have been found in brains of AD patients, so researchers have believed that the incidence of AD is closely related to the accumulation of these plaques in human's brain [16]. In the $A\beta$-lesion hypothesis, it is assumed that amyloid precursor protein (APP) produces sAPPβ and CTFβ through β-secretase, among which the CTFβ is cleaved to form $A\beta$ monomers under catalysis of γ-secretase. Then $A\beta$ monomers further aggregate to form insoluble $A\beta$-plaques, which in turn affects the function of neuronal cells seriously [17]. Experimental and theoretical studies on AD also have elucidated the aggregation process generating the $A\beta$-peptide [2, 3, 16, 17]. In addition, the AD-mouse model showed that the $A\beta$ can cause the increase in cell membrane with permeability, which makes a large amount of Ca^{2+} flow into cytoplasm and destroys the Ca^{2+}-homeostasis in the brain. Increasing evidences suggested that the AD is induced by continuous disturbance of intracellular Ca^{2+} homeostasis in the brain [18, 19]. Berridge showed that the concentration of Ca^{2+} remains high in the neurites near the amyloid deposits, which contributes to the cognitive decline due to long-term depression and temporally memory-storage elimination [20]. Meantime, the excessive Ca^{2+} may lead to the accumulation of $A\beta$ in rat cortical neurons by stimulating the γ-secretase activity, which was also confirmed by the study on the endogenous enzymes in human neuroblastoma SH-SY5Y cells in vitro [21, 22]. These results demonstrated that the permanent increase of Ca^{2+} enhances the γ-secretase activity, thereby improving the production and toxicity of $A\beta$ [23]. Intuitively, we believe that there exists a positive feedback loop between the changes of $A\beta$ and Ca^{2+}: the accumulation of $A\beta$ contributes to the increase of Ca^{2+}, and which in turn improves the level of $A\beta$. This forms a pernicious cycle between the two

sides, and accelerates the development of AD. Caluwé and Dupont [1] firstly proposed a deterministic AD model to formalize the positive feedback loop between $A\beta$ and Ca^{2+}:

$$\begin{aligned}\frac{dx}{dt} &= V_1 + V_3 f(y) - k_1 x,\\ \frac{dy}{dt} &= V_2 + V_4 g(x) - k_2 y,\end{aligned} \tag{1}$$

where x and y denote the concentrations of $A\beta$ and the intracellular Ca^{2+}, respectively. V_1 is the basic synthesis rate of $A\beta$, and k_1 is the clearing rate of $A\beta$. V_2 represents the rate at which Ca^{2+} flow into the cytoplasm, and k_2 is the decay rate of Ca^{2+}. $V_3 f(y)$ denotes the positive feedback of Ca^{2+} acting on $A\beta$ (stimulating the γ-secretase activity), where $f(y) = \frac{y^2}{k_3^2+y^2}$, and k_3 is a half-saturation constant. $V_4 g(x)$ represents the positive feedback of $A\beta$ acting on Ca^{2+} (increasing the permeability of cell membrane), and the concentration of Ca^{2+} changes very quickly in the cell, where $g(x) = x$. Caluwé and Dupont obtained that under a set of appropriate parameters, System (1) has three internal equilibria, E_1 (small), E_2 (middle) and E_3 (large). Where E_1, E_3 are asymptotically stable and E_2 is an unstable saddle point. This shows a bistable phenomenon between stable equilibria and they discussed that the intracellular Ca^{2+} homeostasis is disturbed sufficiently, the Ca^{2+} homeostasis becomes a pathological state, and also explored that presenilin mutation accelerates the development of AD.

In addition, the random error or uncertainty is an inevitable factor in the development of organic tissues and biological systems. However, it is of great significance to consider random effect in the study of dynamic models. For AD in the elderly, there is no clear inheritance pattern and well-identified molecular bases. AD is usually described as a multifactorial disease caused by genetic, epigenetic, environmental and metabolic factors related to aging. Therefore, it is necessary to study the dynamics of stochastic models and explore the possibility that AD may be caused by random disturbances. There are two kinds of stochastic noises in the theoretical studies: the intrinsic noise and the extrinsic one. The former noise is incurred by random changes of biochemical reaction between cells [24], like effects of calcium on γ-secretase activity, nuclear fusion and the changes of cell-membrane permeability, while the latter one is induced by the stochastic changes of intracellular microenvironment for $A\beta$ and Ca^{2+}, such as Na^+, pH value as well as immune cells [25, 26]. Since the intrinsic noise in AD mentioned above is caused by complex random changes of biochemical reactions between cells, meanwhile the pathogenesis of AD is accompanied by highly complex ecological processes, it is a great challenge to consider the intrinsic noise in AD. While the extrinsic noise is caused by random changes in the cellular microenvironment, it can also truly reflect random changes between molecules in the cell, and some works on AD have considered the effect of extrinsic noise on the development of AD, for example, Hu et al. [9, 14][1] proposed two stochastic models of the extrinsic noise (including stochastic PDE) to describe the dynamics of $A\beta$ plaques, $A\beta$ oligomers, PrP^C proteins, and the $A\beta$-x-PrP^C complex which are associated with AD. However, Caluwé and Dupont only considered the deterministic AD model and studied the impact of Ca^{2+} on the development process of AD, but they did not consider the extrinsic noise in the cellular microenvironment, so, in this paper, we introduce extrinsic noise into System (1) established by Caluwé and Dupont to investigate the following stochastic system:

$$\begin{aligned}dx &= \left(V_1 + V_3\frac{y^2}{k_3^2+y^2} - k_1 x\right)dt + \sigma_1 x dB_1(t),\\ dy &= \frac{1}{\varepsilon}(V_2 + V_4 x - k_2 y)dt + \frac{\sigma_2}{\sqrt{\varepsilon}} y dB_2(t),\end{aligned} \tag{2}$$

where $0 < \varepsilon \ll 1$. Due to the time scales of the onset of AD and of Ca^{2+} are in years and seconds or minutes, we add $1/\varepsilon$ to System (2) to keep the time scales of $A\beta$ and Ca^{2+} at the same level. $B_i(t)\,(i = 1, 2)$ are the standard Wiener process and $\sigma_i > 0\,(i = 1, 2)$ denote the intensity of noise. It is very common to study the dynamics of the stochastic systems by constructing ellipses through stochastic sensitivity function technique [27]. For example, Xu et al. [28, 29] considered a stochastic model in which two microorganisms compete for an inhibitory growth-limiting nutrient and explored feedback control of noise-induced extinction. Zhao et al. [30] considered a stochastic model with toxic phytoplankton and patchy aggregation,

[1] PrP^C proteins: Cellular prion proteins. $A\beta$-x-PrP^C: PrP^C binds to $A\beta$ oligomer as a receptor to produce $A\beta$-x-PrP^C complex.

revealed that noise-induced phase transitions may explain blooms. In this paper, we study the positivity, global and ergodic properties of stochastic solutions. The confidence ellipses describing the configurational arrangement of stochastic coexistence equilibria are constructed by stochastic sensitivity function technique [27]. The noise-induced switching between two coexistence equilibria and estimation tipping threshold [31] are investigated.

The main purpose of this paper is as follows. We first focus on the deterministic system (i.e., $\sigma_1 = \sigma_2 = 0$ in (2)), explore the process of AD induced by positive feedback strength (reflected by V_3), and we obtain that the concentrations of $A\beta$ and Ca^{2+} jump from lower steady states (healthy states) to higher ones (pathological states), which is a key index to trigger AD. Moreover, we present two periodically feasible drug strategies to alleviate the AD and screen out more effective one, and confirm that as long as the concentrations of $A\beta$ and Ca^{2+} are adjusted to attraction basin in healthy state through drug treatment, the development of AD can be alleviated. Then, for the stochastic system, we prove uniqueness of global positive solutions and give sufficient conditions for stationary distribution. The most important finding is that phenomenon of the noise-induced phase transition occurs, such as noise induces pathological state to change into healthy state. Therefore, we can control the noise intensity by physics methods to keep $A\beta$ and Ca^{2+} in healthy states, which provides theoretical support for the control of AD in the medical field. Our results provide some new suggestions on how to mitigate the progression of Alzheimer's disease.

The rest of this paper reads as follows. In Sect. 2, we study the deterministic system based on Caluwé and Dupont's system through bifurcation analysis. The dynamical effects of different strategies of drug therapy on the development of AD are explored as well. In Sect. 3, we pay attention to the stochastic system, the uniqueness of global positive solutions and sufficient conditions for stationary distribution are studied. Moreover, the noise-induced switching between two coexistence equilibria and estimation tipping threshold are investigated. A summary is presented, and some future works are discussed in the last section.

2 Bifurcation analysis and drug therapy for AD in deterministic system

In this section, we study the dynamics of the deterministic system (2) without noise, and explore how the positive feedback strength (reflected by V_3) between $A\beta$ and Ca^{2+} affects the development of AD. Under periodic treatment, the effects of different treatment strategies of drugs on the development of AD are investigated as well. In our work, we set the parameter values in System (2),

$$\begin{aligned} &V_1 = 0.25,\ V_2 = 0.11,\ V_3 = 2.89,\ V_4 = 1,\\ &k_1 = 0.35,\ k_2 = 5,\ k_3 = 1,\ \varepsilon = 0.01, \end{aligned} \tag{3}$$

to analyze the dynamics of $A\beta$ and Ca^{2+}.

2.1 Bifurcation analysis

The positive feedback between $A\beta$ and Ca^{2+} may accelerates the probability of $A\beta$ accumulation, leading to the formation of a large number of plaques in the brain of patients [32–34]. It may give rise to neurologic disorders and even neurologic death in the elderly people. To explore the effects of positive feedback between $A\beta$ and Ca^{2+} on AD system, in this subsection we focus on the deterministic system (i.e., $\sigma_1 = \sigma_2 = 0$ in (2)) and take V_3 as bifurcation parameter and sketch bifurcation diagram in Fig. 1. As shown in Fig. 1, when $V_3 < V_3^*$, the deterministic system admits a unique stable equilibrium, the levels of $A\beta$ and Ca^{2+} keep at lower stable branches. Slow positive feedback strength contributes to a healthy state. With the increasing of V_3, the concentrations of $A\beta$ and Ca^{2+} also increase, and the deterministic system undergoes a saddle-node bifurcation at $V_3 = V_3^*$. When V_3 passes the first bifurcation point, the deterministic system has 3 equilibria (two stable nodes and one saddle point, see Appendix) and a bistability region is presented for $V_3 \in (V_3^*, V_3^{**})$. Notice that the evolution paths of $A\beta$ and Ca^{2+} depend on the initial concentrations of $A\beta$ and Ca^{2+}, when the initial concentrations of $A\beta$ and Ca^{2+} are low, the evolution paths of $A\beta$ and Ca^{2+} remain in the lower stable branches (healthy states); if the initial concentrations of $A\beta$ and Ca^{2+} are relatively high, then the evolution paths of $A\beta$ and Ca^{2+} will jump from the lower stable branches (healthy states) to the higher

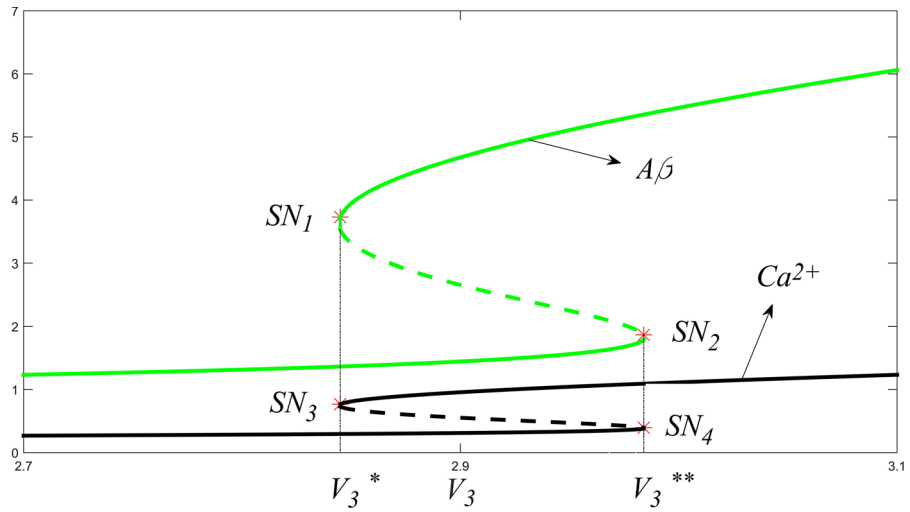

Fig. 1 Bifurcation diagram of the deterministic system with respect to V_3, where $SN_i (i = 1, 2, 3, 4)$ represent saddle-nodes. The green and black curves stand for the concentrations of $A\beta$ and Ca^{2+}, separately. The solid curves represent stable equilibria, and the dotted curves represent unstable equilibria. The proof of asymptotic stability of the equilibria is shown in the appendix. All parameter values are given in (3). (Color figure online)

ones (pathological states). Observe that the healthy and pathological states can switch depending on different levels of initial concentrations of $A\beta$ and Ca^{2+} in the bistable region, we can add human interference to mitigate the development of AD. For example, we can employ drug treatment [3] and physical treatment [35, 36] such that the initial concentrations of $A\beta$ and Ca^{2+} are in the attraction basin of healthy states. As V_3 further increases, a saddle-node bifurcation reoccurs when $V_3 = V_3^{**}$. As V_3 exceeds the threshold V_3^{**}, the deterministic system has a unique stable equilibrium, the levels of $A\beta$ and Ca^{2+} remain at the higher stable branches. The concentrations of $A\beta$ and Ca^{2+} always keep in a pathological state for $V_3 > V_3^{**}$. This transition is reversible, because when the dynamic parameter V_3 decreases, the opposite transition (from high steady state to low steady state) occurs. This shows that even if the levels of $A\beta$ and Ca^{2+} exceed the threshold V_3^{**}, we can reduce the levels of $A\beta$ and Ca^{2+} by human interference.

2.2 Effects of using different strategies for drugs on $A\beta$ and Ca^{2+}

In this subsection, we will explore the impact of different use strategies of the same drugs on AD during periodic treatment. In reality, the patients sometimes change the way of taking drugs at will during the periodic treatment. For example, the doctor originally suggested that the patients should take one dose once a day, but the patients may divide a dose into several parts and take them at equally spaced intervals, then some people question whether the patient's random changes in the way of taking drugs would weaken the effect of relieving AD? To this end, we here investigate the effect of periodic treatment on AD, and whether the patients' random changes in the dosage and the number of times of taking drugs affect the remission of AD. Now we examine the above questions with the help of deterministic system (i.e., $\sigma_1 = \sigma_2 = 0$ in (2)), and use $k_i(t) = a + bsin(t)(i = 1, 2)$ to model periodic drug treatment that can reduce the concentrations of $A\beta$ and Ca^{2+}. Here we assume that the same dose of drugs is used every day, and set up two feasible drug strategies (i) the patients take the drugs once a day at $t \in [6, 7]$ (see Fig. 2a); (ii) the drugs are divided into three parts on average, and the patients take it three times a day at equally spaced intervals $t \in [6, 7]$, $t \in [12, 13]$ and $t \in [18, 19]$ (see Fig. 2b) to relieve the AD. We analyze the dynamics of $A\beta$ and Ca^{2+} within 24 h. As shown in Fig. 2c, d, the blue line represents the absence of periodic treatment, suggesting that it is at the level of disease; the black curve represents the effect of strategy (i); the red curve indicates the effect of strategy (ii). In fact, the concentrations of $A\beta$ and Ca^{2+} have always been in a pathological state without periodic treatment, similar to the concentration of the high stable branch (see Fig. 1); observe that no matter what kind of periodic treatment strategy, the pathological state changes to a healthy state in the form of pulse, that is, the high concentration jumps to a low

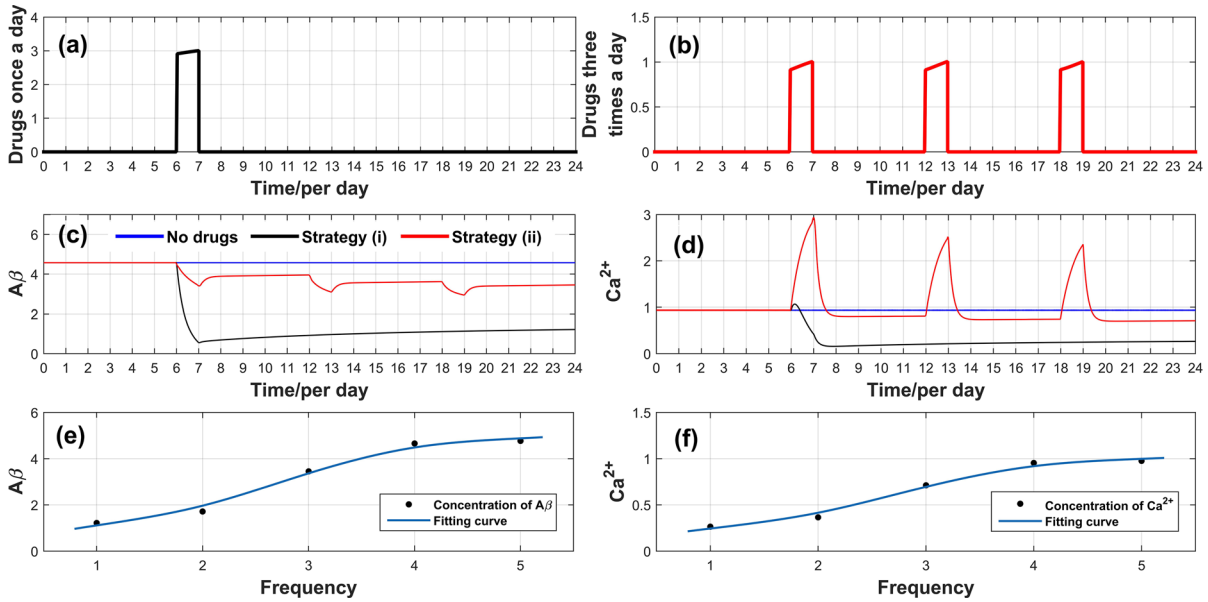

Fig. 2 The effect of drug treatment on the concentrations of $A\beta$ and Ca^{2+}. **a** The patients take the drugs once a day, where $a = 3, b = 0.1$; **b** The drugs are divided into three parts on average, and the patients take them three times a day, where $a = 0.94, 0.965$ and $0.9895, b = 0.1$; **c**, **d** denote the effects of different strategies on the concentrations of $A\beta$ and Ca^{2+}, in which the blue line indicates that no drugs are taken, suggesting that it is at the level of disease, the black curve represents the effect of strategy (i) and the red curve indicates the effect of strategy (ii); **e**, **f** are respectively the final concentrations of $A\beta$ and Ca^{2+} after each evenly divided drug, in which the horizontal axis values show times/frequency that the drugs are evenly divided, the vertical axis values are the stable concentration of $A\beta$ or Ca^{2+} (see solid black dots), here only one to five times/frequency are shown. All parameter values are given in (3)

concentration, similar to the concentration of the jump to the low stable branch (see Fig. 1). It is further found that the amplitude of the concentration reduction of strategy (i) is very large, and the treatment effect is more obvious on alleviating AD compared with strategy (ii). Moreover, we find that for strategy (ii), the concentration of Ca^{2+} decreases in the form of an upward pulse, we suspect that this may be due to the reduction of drug dose in strategy (ii), which leads to the weakening of the effect of alleviating AD, so that it could not produce a positive effect in a short time, and the concentration of Ca^{2+} in cells changes rapidly in seconds or minutes [1], which may cause the concentration of Ca^{2+} to decrease in the form of an upward pulse. In order to display the concentrations of $A\beta$ and Ca^{2+} in the brain of patients after multiple drug use, we take out the concentration values of $A\beta$ and Ca^{2+} for final solution stability after each drugs division and draw Fig. 2e-f, in which the horizontal axis values show times / frequency that the drugs are evenly divided, the vertical axis values are the stable concentration of $A\beta$ or Ca^{2+}(see solid black dots). We can see that the concentrations of $A\beta$ and Ca^{2+} gradually increase with the increase in drugs equalization times/frequency in Fig. 2e, f. This shows that the same dose of drugs is divided into multiple doses, which will slow down the patient's recovery process, it also reflects that strategy (i) is the optimal treatment scheme, that is, here the best treatment effect can be achieved by using three units of medicine once at $t \in [6, 7]$ every day. Thus, we conclude that periodic treatment can significantly alleviate AD, and the effect of relieving AD will be slower if the patients change the way of taking medicine at will. This indirectly reflects that following the doctor's advice and taking drugs scientifically play an important role in the recovery of the patients.

Remark 1 Notice that in System (2), let $\sigma_1 = \sigma_2 = 0$, we have already guaranteed that time scales of $A\beta$ and Ca^{2+} is the same level (the right-hand side of the second equation of System (2) is multiplied by $\frac{1}{\varepsilon}$ $(0 < \varepsilon \ll 1)$), so without loss of generality, we draw (c) and (d) in hours with a step length of 0.01 by using ODE45 command in MATLAB 2014. We here

chose the periodic function $k_i(t) = a + b\ \sin(t)$ as the quantity of the drugs, whereas the quantity of the drugs can also be described by other functions, as long as these functions can simulate a periodic curve greater than zero.

Remark 2 Figure 2 shows the effect of different strategies of periodic drug therapy on the progression of AD. The drugs on the market for the treatment of AD, such as galantamine, donepezil, rivastigmine, memantine and herbal medicine, can alleviate the development of AD to a certain extent by inhibiting acetylcholine, but these drugs may also produce certain side effects, such as diarrhea, nausea and vomiting. Few patients also experience life-threatening adverse effects such as thrombocytopenia, heart attack, adenocarcinoma and extreme anaemia. In addition, various different and contradictory assumptions have made it difficult to determine the exact mechanism and physiological function of the disease itself, as well as the obstacles of drug transport across the impenetrable blood–brain barrier. Additionally, due to the inability to target the large area of neuron and synaptic death in AD brain, the current treatment has also reached a bottleneck. Moreover, Tatiaparti et al. [37] have suggested that so far, more than 200 AD clinical trials have failed. One of these failures is irreversible damage to the patient's neurons, leaving little scope for the use of different drugs, which makes drug treatment of AD particularly difficult. Thus, in order to seek promising therapeutic measures for the treatment of AD, more scholars focus on neurology [38, 39] because AD is a neurological disease, and some studies have presented physical therapy methods to affect the brain nerves of patients to achieve the purpose of treating AD [36, 40]. Therefore, in the second half, we will establish a stochastic system about AD. We take random disturbances in System as control variables, such as language training, physical therapy, to realize the control of AD so as to slow the deterioration of AD.

In summary, the positive feedback between $A\beta$ and Ca^{2+} produces bistability, that is, the evolution of AD can be described as a bistable transition. The initial value concentrations of $A\beta$ and Ca^{2+} can be adjusted to the basin attraction of low steady state through human intervention, which can slow down the development of AD even if the levels of $A\beta$ and Ca^{2+} exceed the threshold V_3^{**}. In addition, we give two periodic treatment strategies for AD remission, which provides guidance for the scientific use of drugs in AD patients.

3 Analysis of the stochastic system

Notice that the evolution paths of $A\beta$ and Ca^{2+} in bistability region depend on the initial concentrations of $A\beta$ and Ca^{2+}. In this bistability region, stochastic variations in the microenvironment of $A\beta$ and Ca^{2+} may easily change the concentrations of $A\beta$ and Ca^{2+}. In this section, we explore how the extrinsic noise from stochastic variations of microenvironment for $A\beta$ and Ca^{2+} in the bistability region affects the development of AD. We discuss the uniqueness of global positive solutions and the existence of unique stationary distribution, and the noise-induced switching between two coexistence equilibria of the stochastic system (2). In our work, we choose different noise intensities to study the dynamics of $A\beta$ and Ca^{2+} and adopt the Milstein's higher order method [41] in our numerical simulations.

3.1 Stationary distribution

In this subsection, we intend to present that there exists a unique ergodic stationary distribution. We first prove that the stochastic system (2) has a unique global positive solution.

Let $z(t)$ be a time-homogeneous Markov process in E_d (d-dimensional Euclidean space), which is represented by the following equation:

$$\mathrm{d}z(t) = h(z)\mathrm{d}t + \sum_{r=1}^{k} g_r(z)\mathrm{d}B_r(t),$$

where $h(z) = (h_1(z), h_2(z), \ldots, h_d(z)), g_r(z) = (g_r^1(z), g_r^2(z), \ldots, g_r^d(z))$ and $B_r(t)\ (r = 1, 2, \ldots, k)$ are independent standard Brownian motions defined on some probability space (Ω, F, P). Let $A(z)$ be the diffusion matrix, which is written as the following form

$$A(z) = (a_{ij}(z))_{d\times d}, \quad a_{ij}(z) = \sum_{r=1}^{k} g_r^i(z) g_r^j(z).$$

Now, we state a lemma to show that System (2) has a stationary distribution.

Lemma 1 (*see* [42, 43]) *Assume that there exists a bounded domain $D \subset E_d$ with regular boundary, satisfying the following properties.*

(i) In the domain D and some neighborhood thereof, the smallest eigenvalue of the diffusion matrix $A(z)$ is bounded away from zero.

(ii) If $z \in E_d \backslash D$, the mean time τ at which a path issuing from z reaches the set D is finite, and $\sup_{z\in K} E_z\tau < \infty$ for every compact subset $K \subset E_d$.

Then, the Markov process $z(t)$ has a stationary distribution $\mu(\cdot)$ with density in E_d such that $\lim_{t\to\infty} P\{z(t) \in B\} = \mu(B)$ for any Borel set $B \subset E_d$, and

$$P\left\{\lim_{T\to\infty}\frac{1}{T}\int_0^T f(z(t))\mathrm{d}t = \int_{E_d} f(z)\mu(\mathrm{d}z)\right\} = 1,$$

for all $z \in E_d$, where $f(z)$ is a function integrable with respect to the measure μ.

Remark 3 To verify condition (i), it is sufficient to show that there exists a positive constant G such that $\sum_{i,j=1}^d a_{ij}(z)\xi_i\xi_j \geq G|\xi|^2, z \in D, \xi \in R^d$(see [44, 45]). To validate condition (ii), it is sufficient to show that there is a nonnegative C^2-function $H(z)$ and a bounded domain $D \subset E_d$ with regular boundary such that for some constant k one has $LH(z) < -k$ for all $z \in E_d \backslash D$ (see [46]).

Theorem 1 *For any given initial value $(x_0, y_0) \in R_+^2$, $t \geq 0$, System (2) admits a unique solution $(x(t), y(t))$, which remains in R_2^+ with probability one.*

Proof Observe that the coefficients of System (2) satisfy the local Lipschitz conditions, then System (2) admits a unique local solution $(x(t), y(t))$ for $t \in [0, \tau_e)$, where τ_e is explosion time. Now we show that the solution exists globally, i.e., $\tau_e = +\infty$ almost surely (a.s.). For any initial value, there exists a sufficiently large $n_0 \geq 1$ such that $x_0, y_0 \in \left[\frac{1}{n_0}, n_0\right]$. For each integer $n > n_0$, we give a following stopping time:

$$\tau_n = \inf\left\{t \in [0, \tau_e) : \min\{x, y\} \leq \frac{1}{n} \text{ or } \max\{x, y\} \geq n\right\}.$$

Here, we define $\inf \emptyset = \infty$ ($\emptyset$ represents empty set). Obviously, τ_n increases as $n \to \infty$. Choose $\tau_\infty = \lim_{n\to+\infty} \tau_n$, then $\tau_\infty \leq \tau_e$ a.s., thus, we only need to obtain that $\tau_\infty = \infty$ a.s. Assume that $\tau_\infty = \infty$ is untrue, then we find two constants $T > 0$ and $\zeta \in (0, 1)$ such that $P\{\tau_\infty \leq T\} > \zeta$. Therefore, there exists $n_1 \geq n_0$ ($n_1 \in N_+$) such that

$$P\{\tau_n \leq T\} \geq \zeta, n \geq n_1.$$

Define a C^2-function $U : R_2^+ \to R_+$ as

$$U(x, y) = \frac{V_4}{\varepsilon k_1}(x - 1 - \ln x) + (y - 1 - \ln y).$$

It is easy to see that $U(x, y) \geq 0$ for any $(x, y) \in R_2^+$. By Itô's formula, we have

$$\begin{aligned}\mathrm{d}U(x, y) = {} & LU(x, y)\mathrm{d}t + \frac{V_4\sigma_1}{\varepsilon k_1}(x - 1)\mathrm{d}B_1 \\ & + \frac{\sigma_2}{\sqrt{\varepsilon}}(y - 1)\mathrm{d}B_2,\end{aligned}$$

where

$$\begin{aligned}LU = {} & \frac{V_4}{\varepsilon k_1}\left(V_1 + \frac{V_3y^2}{k_3^2 + y^2} - k_1x - \frac{V_1}{x} - \frac{V_3y^2}{x(k_3^2 + y^2)} + k_1\right) \\ & + \frac{1}{\varepsilon}\left(V_2 + V_4x - k_2y - \frac{V_2}{y} - \frac{V_4}{y}x + k_2\right) + \frac{1}{2}\left(\frac{V_4\sigma_1^2}{\varepsilon k_1} + \frac{\sigma_2^2}{\varepsilon}\right) \\ \leq {} & \frac{V_4}{\varepsilon k_1}(V_1 + V_3 - k_1x + k_1) + \frac{1}{\varepsilon}(V_2 + V_4x + k_2) + \frac{1}{2}\left(\frac{V_4\sigma_1^2}{\varepsilon k_1} + \frac{\sigma_2^2}{\varepsilon}\right) \\ = {} & \frac{V_4}{\varepsilon k_1}(V_1 + V_3 + k_1) + \frac{1}{\varepsilon}(V_2 + k_2) + \frac{1}{2}\left(\frac{V_4\sigma_1^2}{\varepsilon k_1} + \frac{\sigma_2^2}{\varepsilon}\right) \\ := {} & K_0.\end{aligned}$$

Thus,

$$\mathrm{d}U(x, y) \leq K_0\mathrm{d}t + \frac{V_4\sigma_1}{\varepsilon k_1}(x - 1)\mathrm{d}B_1 + \frac{\sigma_2}{\sqrt{\varepsilon}}(y - 1)\mathrm{d}B_2.$$

Integrating this inequality on both sides from 0 to $\tau_n \wedge T$ and taking expectation, we have

$$\begin{aligned}EU(x(\tau_n \wedge T), y(\tau_n \wedge T)) & \leq U(x(0), y(0)) + E\int_0^{\tau_n\wedge T} K_0\mathrm{d}t \\ & \leq U(x(0), y(0)) + K_0T.\end{aligned}$$

Define $\Omega_n = \{\tau_n \leq T\}$ for any integer $n > n_1$, we can obtain $P\{\Omega_n\} \geq \zeta$. So, at least one of $x(\tau_n, \omega)$ or $y(\tau_n, \omega)$ is always equal to n or $\frac{1}{n}$ for any $\omega \in \Omega_n$. Thus

$$U(x(\tau_n, \omega), y(\tau_n, \omega)) \geq \min\left[\frac{1}{n} - 1 - \ln\frac{1}{n}, n - 1 - \ln n\right].$$

Then we have

$$U(x(0),y(0))+K_0T\geq E[1_{\Omega_n(\omega)}U(x(\tau_n,\omega),y(\tau_n,\omega))]$$
$$\geq\zeta\cdot\min\left[\frac{1}{n}-1-\ln\frac{1}{n},n-1-\ln n\right],$$

where $1_{\Omega_n(\omega)}$ denotes the indicative function of Ω_n. Let $n\to\infty$, we obtain

$$\infty>U(x(0),y(0))+K_0T\geq\zeta\cdot\min\left[\frac{1}{n}-1-\ln\frac{1}{n},n-1-\ln n\right]=\infty,$$

which contradicts the fact. Therefore, we obtain $\tau_\infty=\infty$ a.s. This completes the proof of Theorem 1.

Let

$$\Lambda=\min\left\{k_1-\frac{V_4}{N\varepsilon},\frac{k_2}{\varepsilon}\right\}-\frac{\theta}{2}\max\left\{\sigma_1^2,\frac{\sigma_2^2}{\varepsilon}\right\},\left(k_1>\frac{V_4}{N\varepsilon}\right).\tag{4}$$

Theorem 1 guarantees that the concentrations of $A\beta$ and Ca^{2+} of System (2) are positive and global, which is essential to illustrate that System (2) has a unique ergodic stationary distribution and satisfies the condition (4).

Theorem 2 *Assume that* $k_1>\frac{V_4}{N\varepsilon}$, $\Lambda>0$ *for* $N>0$ *and* $0<\theta<1$. *Then for any given initial value* $(x_0,y_0)\in R_+^2$, *System* (2) *admits a unique stationary distribution.*

Proof. The proof is divided into two steps, we first verify condition (i) in the Lemma 1 holds. It is easy to obtain the diffusion matrix of System (2):

$$A=\begin{pmatrix}\sigma_1^2x^2 & 0\\ 0 & \frac{\sigma_2^2}{\varepsilon}y^2\end{pmatrix}=(a_{ij}).$$

Define $G=\min_{(x,y)\in D_k\subset R_+^2}\left\{\sigma_1^2x^2,\frac{\sigma_2^2}{\varepsilon}y^2\right\}$ and $D_k=\left[\frac{1}{k},k\right]\times\left[\frac{1}{k},k\right]$ for sufficiently large integer $k>0$. For any $(x,y)\in D_k$ and $\xi=(\xi_1,\xi_2)\in R^2$, we have

$$\sum_{i,j=1}^{2}a_{ij}\xi_i\xi_j=a_{11}\xi_1\xi_1+a_{22}\xi_2\xi_2=\sigma_1^2x^2\xi_1^2+\frac{\sigma_2^2}{\varepsilon}y^2\xi_2^2\geq\min\left\{\sigma_1^2x^2,\frac{\sigma_2^2}{\varepsilon}y^2\right\}\left[\xi_1^2+\xi_2^2\right]=G\|\xi^2\|.$$

Therefore, condition (i) in Lemma 1 holds.

Next, we show that the condition (ii) of Lemma 1 holds. By the Itô's formula, we have

$$L[-Nx-y-\ln y]=-N\left(V_1+\frac{V_3y^2}{k_3^2+y^2}-k_1x\right)-\frac{1}{\varepsilon}(V_2+V_4x-k_2y)-\frac{1}{\varepsilon}\left(\frac{V_2}{y}+\frac{V_4x}{y}-k_2\right)+\frac{\sigma_2^2}{2\varepsilon},$$

and

$$\begin{aligned}
&L\left(\frac{1}{\theta+1}(Nx+y)^{\theta+1}\right)=(Nx+y)^{\theta}\left(NV_1+\frac{NV_3y^2}{k_3^2+y^2}-k_1Nx+\frac{1}{\varepsilon}(V_2+V_4x-k_2y)\right)\\
&+\frac{\theta}{2}(Nx+y)^{\theta-1}\left(\sigma_1^2N^2x^2+\frac{\sigma_2^2}{\varepsilon}y^2\right)\\
&\leq(Nx+y)^{\theta}\left(NV_1+NV_3+\frac{V_2}{\varepsilon}-\min\left\{k_1-\frac{V_4}{N\varepsilon},\frac{k_2}{\varepsilon}\right\}(Nx+y)\right)\\
&+\frac{\theta}{2}(Nx+y)^{\theta+1}\max\left\{\sigma_1^2,\frac{\sigma_2^2}{\varepsilon}\right\}\\
&=(Nx+y)^{\theta}\left(NV_1+NV_3+\frac{V_2}{\varepsilon}\right)-(Nx+y)^{\theta+1}\min\left\{k_1-\frac{V_4}{N\varepsilon},\frac{k_2}{\varepsilon}\right\}\\
&+\frac{\theta}{2}(Nx+y)^{\theta+1}\max\left\{\sigma_1^2,\frac{\sigma_2^2}{\varepsilon}\right\}\\
&=(Nx+y)^{\theta}\left(NV_1+NV_3+\frac{V_2}{\varepsilon}\right)-\Lambda(Nx+y)^{\theta+1}\\
&=C-\frac{\Lambda}{2}(Nx+y)^{\theta+1}\leq C-\frac{\Lambda}{2}(x^{\theta+1}+y^{\theta+1}),
\end{aligned}$$

where

$C=(Nx+y)^{\theta}\left(NV_1+NV_3+\frac{V_2}{\varepsilon}\right)-\frac{\Lambda}{2}(Nx+y)^{\theta+1}$.

There exist two positive constants N and $0<\theta<1$ such that $k_1>\frac{V_4}{N\varepsilon}$ and $\Lambda>0$. Choosing a C^2-function

$$H=(-Nx-y-\ln y)+\frac{1}{\theta+1}(Nx+y)^{\theta+1},$$

then

$$\lim_{k\to\infty,(x,y)\in R_+^2\setminus D_k}\inf H(x,y)=\infty,$$

here $D_k=\left(\frac{1}{k},k\right)\times\left(\frac{1}{k},k\right)$ with integer $k>1$. Since $H(x,y)$ is a continuous function, it admits a minimum value $H(x_0,y_0)$ in R_+^2. Then we get the following nonnegative C^2- function

$$H=(-Nx-y-\ln y)+\frac{1}{\theta+1}(Nx+y)^{\theta+1}-H(x_0,y_0),$$

thus

$$
\begin{aligned}
LH \le & C - \frac{\Lambda}{2}(x^{\theta+1} + y^{\theta+1}) - N\left(V_1 + \frac{V_3 y^2}{k_3^2 + y^2} - k_1 x\right) - \frac{1}{\varepsilon}(V_2 + V_4 x - k_2 y) \\
& - \frac{1}{\varepsilon}\left(\frac{V_2}{y} + \frac{V_4 x}{y} - k_2\right) + \frac{\sigma_2^2}{2\varepsilon}, \\
\le & C - \frac{\Lambda}{2}(x^{\theta+1} + y^{\theta+1}) - \left(NV_1 + \frac{V_2}{\varepsilon}\right) + \frac{k_2}{\varepsilon} + \frac{\sigma_2^2}{2\varepsilon} + N\left(k_1 - \frac{V_4}{N\varepsilon}\right)x \\
& + \frac{k_2}{\varepsilon} y - \frac{V_2}{\varepsilon y} - \frac{V_4}{\varepsilon y} x.
\end{aligned}
$$

To show condition (ii) in Lemma 1 holds, we construct a compact subset Ω. Define

$$
\Omega = \left\{ (x, y) \in R_+^2 \,\middle|\, \delta_1 \le x \le \frac{1}{\delta_1}, \delta_2 \le y \le \frac{1}{\delta_2} \right\},
$$

where $\delta_i > 0 (i = 1, 2)$ are sufficiently small constants.

For the convenience, we set

$$
\begin{aligned}
&\Omega_1 = \{(x, y) \in R_+^2 | 0 < x < \delta_1\}, \quad \Omega_2 = \{(x, y) \in R_+^2 | 0 < y < \delta_2, x \ge \delta_1\}, \\
&\Omega_3 = \left\{ (x, y) \in R_+^2 \,\middle|\, x \ge \frac{1}{\delta_1} \right\}, \quad \Omega_4 = \left\{ (x, y) \in R_+^2 \,\middle|\, y \ge \frac{1}{\delta_2} \right\}.
\end{aligned}
$$

Obviously, $R_+^2 \backslash \Omega = \cup_{i=1}^4 \Omega_i$. Now we need to prove that $LH(x, y) \le -1$ on $R_+^2 \backslash \Omega$, which is equivalent to show $LH(x, y) \le -1$ holds on the $\Omega_i (i = 1, 2, 3, 4)$.

Case 1 If $(x, y) \in \Omega_1$, then.

$$
LH \le F_1 - \left(NV_1 + \frac{V_2}{\varepsilon}\right) + N\left(k_1 - \frac{V_4}{N\varepsilon}\right)\delta_1,
$$

where $F_1 = \sup_{(x,y) \subset R_+^2} \{C - \frac{\Lambda}{2}(x^{\theta+1} + y^{\theta+1}) + \left(\frac{k_2}{\varepsilon} + \frac{\sigma_2^2}{2\varepsilon}\right) + \frac{k_2}{\varepsilon} y\}$.

Then there exists a sufficiently small constant $\delta_1 > 0$ and sufficiently large constant $N > 0$ such that $F_1 - \left(NV_1 + \frac{V_2}{\varepsilon}\right) + N\left(k_1 - \frac{V_4}{N\varepsilon}\right)\delta_1 < -1$, thus we have

$$
LH \le -1 \text{ for all } (x, y) \in \Omega_1.
$$

Case 2 If $(x, y) \in \Omega_2$, then

$$
LH \le F_2 + \frac{k_2}{\varepsilon}\delta_2 - \frac{1}{\varepsilon\delta_2}(V_2 + V_4\delta_1),
$$

where

$$
F_2 = \sup_{(x,y) \subset R_+^2} \left\{ C - \frac{\Lambda}{2}(x^{\theta+1} + y^{\theta+1}) - \left(NV_1 + \frac{V_2}{\varepsilon}\right) + \frac{k_2}{\varepsilon} + \frac{\sigma_2^2}{2\varepsilon} + N\left(k_1 - \frac{V_4}{N\varepsilon}\right)x \right\}.
$$

Then there exists a sufficiently small constant $\delta_2 > 0$ such that $F_2 + \frac{k_2}{\varepsilon}\delta_2 - \frac{1}{\varepsilon\delta_2}(V_2 + V_4\delta_1) < -1$, hence, we know

$$
LH \le -1 \text{ for all } (x, y) \in \Omega_2.
$$

Case 3 If $(x, y) \in \Omega_3$, then

$$
LH \le F_3 - \frac{\Lambda}{2}\left(\frac{1}{\delta_1}\right)^{\theta+1},
$$

where $F_3 = \sup_{(x,y) \subset R_+^2} \{C - \left(NV_1 + \frac{V_2}{\varepsilon}\right) + \frac{k_2}{\varepsilon} + \frac{\sigma_2^2}{2\varepsilon} + N\left(k_1 - \frac{V_4}{N\varepsilon}\right)x + \frac{k_2}{\varepsilon} y\}$.

Then there exists a sufficiently small constant $\delta_1 > 0$ such that $F_3 - \frac{\Lambda}{2}\left(\frac{1}{\delta_1}\right)^{\theta+1} < -1$, we can get

$$
LH \le -1 \text{ for all } (x, y) \in \Omega_3.
$$

Case 4 If $(x, y) \in \Omega_4$, then we can obtain

$$
LH \le F_3 - \frac{\Lambda}{2}\left(\frac{1}{\delta_2}\right)^{\theta+1}.
$$

There exists a sufficiently small constant $\delta_2 > 0$ such that $F_3 - \frac{\Lambda}{2}\left(\frac{1}{\delta_2}\right)^{\theta+1} < -1$, we obtain that

$$
LH \le -1 \text{ for all } (x, y) \in \Omega_4.
$$

From the above analysis of four cases, we can achieve

$$
LH(x, y) \le -1, \text{ for all } (x, y) \in R_+^2 \backslash \Omega,
$$

which completes the proof.

Theorem 2 shows that if the initial concentrations of $A\beta$ and Ca^{2+} are greater than 0 and the conditions of Theorem 2 hold, then System (2) has a unique ergodic stationary distribution. Here, we adopt the Milstein's higher order method to obtain the corresponding discrete equations as follows:

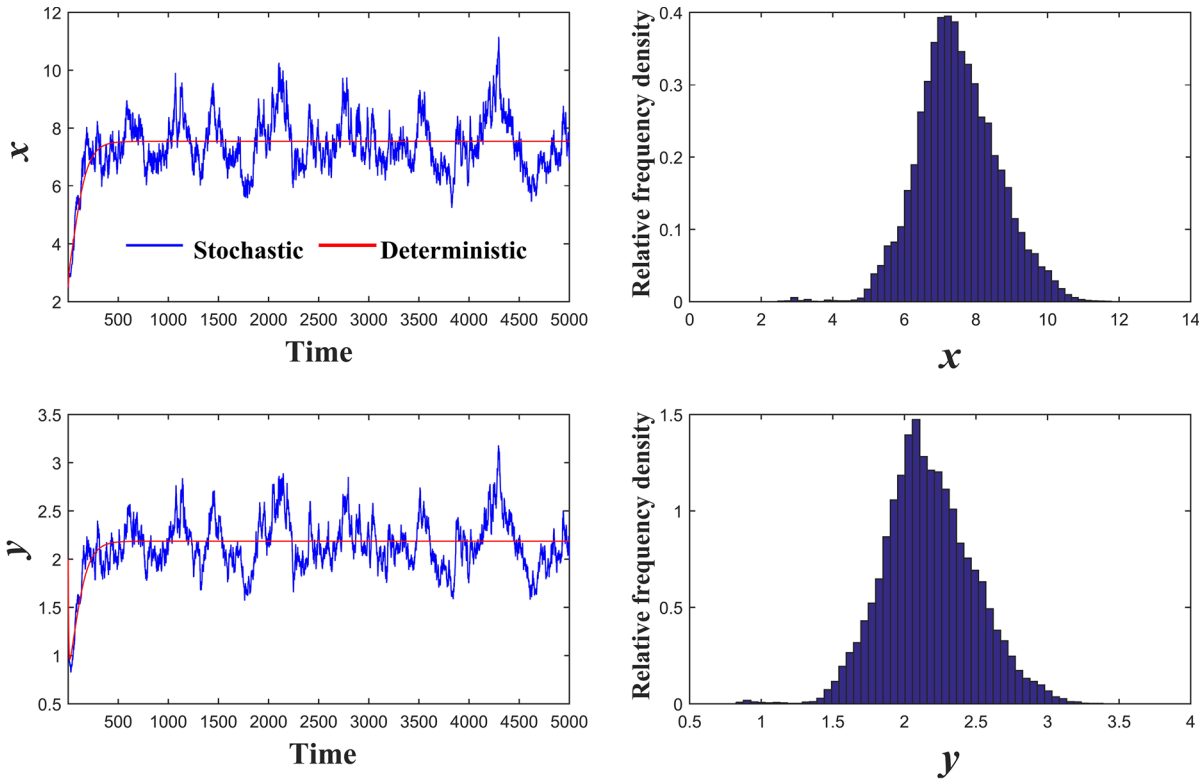

Fig. 3 The left subfigures are the evolution paths of x and y for System (1) and System (2) with initial values (2.5, 2). The right subfigures show histograms of probability density function of x and y. Here, $\sigma_1 = 0.1, \sigma_2 = 0.08, k_2 = 3.5, \theta = 0.2, N = 1000$ and other parameter values are given in (3), and $\Lambda = 0.1860$.

$$x_{i+1} = x_i + \left(V_1 + V_3\frac{y_i^2}{k_3^2 + y_i^2} - k_1 x_i\right)\Delta_t + x_i\left[\sigma_1\xi_i\sqrt{\Delta_t} + \frac{1}{2}\sigma_1^2(\xi_i^2 - 1)\Delta_t\right],$$
$$y_{i+1} = y_i + \frac{1}{\varepsilon}(V_2 + V_4 x_i - k_2 y_i)\Delta_t + \frac{y_i}{\sqrt{\varepsilon}}\left[\sigma_2\xi_i\sqrt{\Delta_t} + \frac{1}{2}\sigma_2^2(\xi_i^2 - 1)\Delta_t\right],$$

where $\xi_i\ (i = 1, 2, \ldots)$ are Gaussian random variables and follow the standard normal distribution $N(0, 1)$. Here, we take $\sigma_1 = 0.1, \sigma_2 = 0.08, k_2 = 3.5, \theta = 0.2, N = 1000$ and then $\Lambda = 0.1860$. The numerical simulations shown in Fig. 3 illustrate that System (2) exhibits a unique ergodic stationary distribution. This also shows that AD will persist.

3.2 Analysis of transition between two coexistence equilibria induced by noise

According to work of Caluwé and Dupont and (3), System (1) admits three equilibria, $E_1 = (1.4282, 0.3076), E_2 = (2.7517, 0.5723)$ and $E_3 = (4.5716, 0.9363)$, where E_2 is an unstable saddle point, both E_1 and E_3 are asymptotically stable (see Appendix). Attractive domains of the stable equilibria

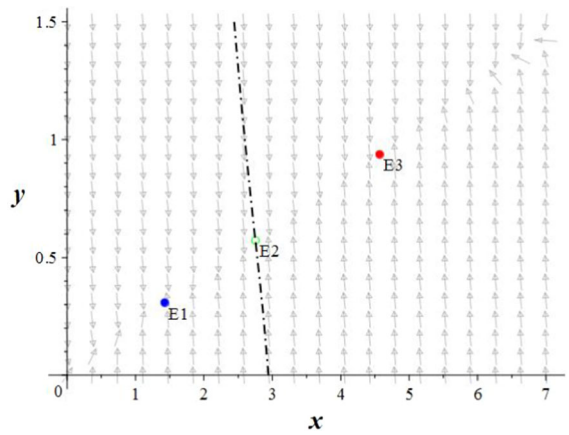

Fig. 4 Vector field of System (1), and the black dash-dotted line represents the separatrix between the attraction basins of two coexistence equilibria (E_1 and E_3). Solid dots represent stable equilibria (blue and red), and hollow dot represents unstable saddle point (green). The approximate equation of the separatrix is $y = -2.976x + 8.7614$. (Color figure online)

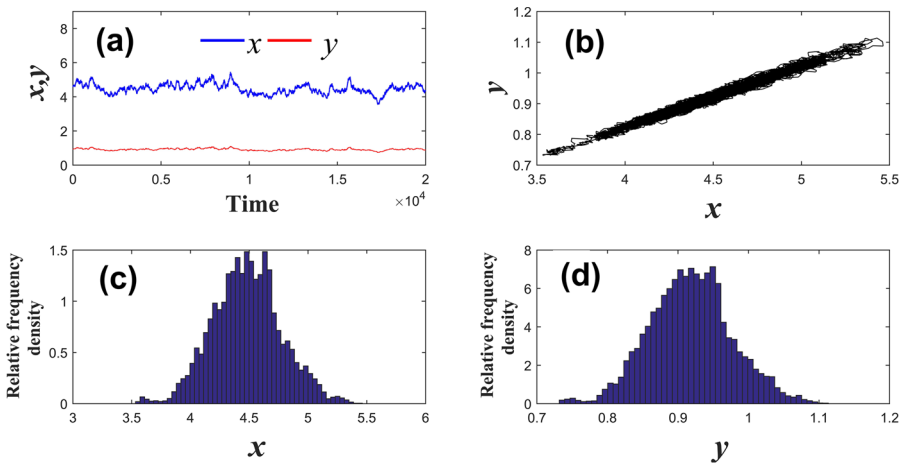

Fig. 5 **a** Time series diagram of System (2); **b** Phase trajectory of System (2) with the initial value $(4.5716, 0.9363)$ and the noise intensity $\sigma_1 = \sigma_2 = 0.02$; **c**, **d** show histograms of probability density function of x and y. Other parameter values are given in (3)

are separated by the stable manifold of the saddle, which shows a bistable phenomenon between stable equilibria (see Fig. 4). In this subsection, we will estimate the tipping threshold [31] and explore the switch between two coexistence equilibria (E_1 and E_3) via stochastic sensitivity function technique [27], which are both induced by noise.

In Fig. 4, we plot the vector field of the deterministic system, in which the black dash-dotted line represents the separatrix between the attraction basins of two coexistence equilibria (E_1 and E_3). Equilibrium E_3 is a pathological state and E_1 is a healthy state. As can be seen in Fig. 4, the initial values are chosen in the attraction basin (the right (left) area of separatrix) of $E_3(E_1)$, and the trajectories starting from these initial values eventually converge to the equilibrium $E_3(E_1)$. However, the stochastic system sometimes cannot accurately predict its dynamics. In order to study how environmental noise affects dynamics of System (2) and estimate tipping threshold, we set $\sigma = \sigma_1 = \sigma_2$ and take E_3 as an example in System (2). As presented in Fig. 5, when the noise intensity is quite small ($\sigma_1 = \sigma_2 = 0.02$), the random trajectories starting from the attraction basin of E_3 finally oscillate slightly near the equilibrium E_3, and the concentrations of $A\beta$ and Ca^{2+} oscillate around the constant level. From Fig. 6, we observe that as the noise intensity increases, large noise intensity ($\sigma_1 = \sigma_2 = 0.5$) makes the random trajectories starting from the attraction basin of E_3 eventually cross the separatrix and reach the surroundings of equilibrium E_1 or tend to zero. Large noise intensity makes the concentrations of $A\beta$ and Ca^{2+} decrease to the lowest, and even tend to zero.

Next, we construct the confidence ellipses to describe the configurational arrangement of stochastic equilibria using stochastic sensitivity function technique [27], and further estimate tipping threshold σ.

Define

$$F = \begin{pmatrix} f_{11} & f_{12} \\ f_{21} & f_{22} \end{pmatrix}, G = \begin{pmatrix} g_{11} & 0 \\ 0 & g_{22} \end{pmatrix}, S = GG^T,$$

where $f_{11} = -k_1, f_{12} = \frac{2V_3 y}{k_3^2+y^2} - \frac{2V_3 y^3}{(k_3^2+y^2)^2}, f_{21} = \frac{V_4}{\varepsilon}, f_{22} = -\frac{k_2}{\varepsilon}, g_{11} = x, g_{22} = \frac{y}{\sqrt{\varepsilon}}$.

Let W be the stochastic sensitivity matrix:

$$W = \begin{pmatrix} \omega_{11} & \omega_{12} \\ \omega_{21} & \omega_{22} \end{pmatrix},$$

which satisfies the following equations:

$$\begin{cases} 2f_{11}\omega_{11} + f_{12}\omega_{12} + f_{12}\omega_{21} = -g_{11}^2, \\ f_{21}\omega_{11} + (f_{11} + f_{22})\omega_{12} + f_{12}\omega_{22} = 0, \\ f_{21}\omega_{11} + (f_{11} + f_{22})\omega_{21} + f_{12}\omega_{22} = 0, \\ f_{21}\omega_{12} + f_{21}\omega_{21} + 2f_{22}\omega_{22} = -g_{22}^2. \end{cases}$$

From (A.3) in [27], we have the following confidence ellipse equation

$$\langle (x-\overline{x}, y-\overline{y})^T, W^{-1}(x-\overline{x}, y-\overline{y})^T \rangle = 2\sigma^2 \log\left(\frac{1}{1-P}\right), \tag{5}$$

where σ and P are the noise intensity and fiducial probability, separately. $(\overline{x}, \overline{y})$ is a positive equilibrium of the deterministic system (1).

At $E_1 = (1.4282, 0.3076)$, we obtain the stochastic sensitivity matrix and its inverse,

$$W_1 = \begin{pmatrix} 19.1039 & 3.8189 \\ 3.8189 & 0.7732 \end{pmatrix}, W_1^{-1} = \begin{pmatrix} 4.1132 & -20.3144 \\ -20.3144 & 101.6222 \end{pmatrix}.$$

From (5), the confidence ellipse equation at equilibrium E_1 is given by

$$\begin{aligned} &4.1132(x-1.4282)^2 - 40.6288(x-1.4282) \\ &(y-0.3076) + 101.6222(y-0.3076)^2 \\ &= 2\sigma_1^2 \log\left(\frac{1}{1-P_1}\right). \end{aligned} \tag{6}$$

The stochastic sensitivity matrix and its inverse at $E_3 = (4.5716, 0.9363)$ read as

$$W_3 = \begin{pmatrix} 244.1360 & 48.8081 \\ 48.8081 & 9.8493 \end{pmatrix}, W_3^{-1} = \begin{pmatrix} 0.4406 & -2.1835 \\ -2.1835 & 10.9216 \end{pmatrix}.$$

By (5), we obtain the confidence ellipse equation at equilibrium E_3

$$\begin{aligned} &0.4406(x-4.5716)^2 - 4.367(x-4.5716) \\ &(y-0.9363) + 10.9216(y-0.9363)^2 \\ &= 2\sigma_2^2 \log\left(\frac{1}{1-P_2}\right). \end{aligned} \tag{7}$$

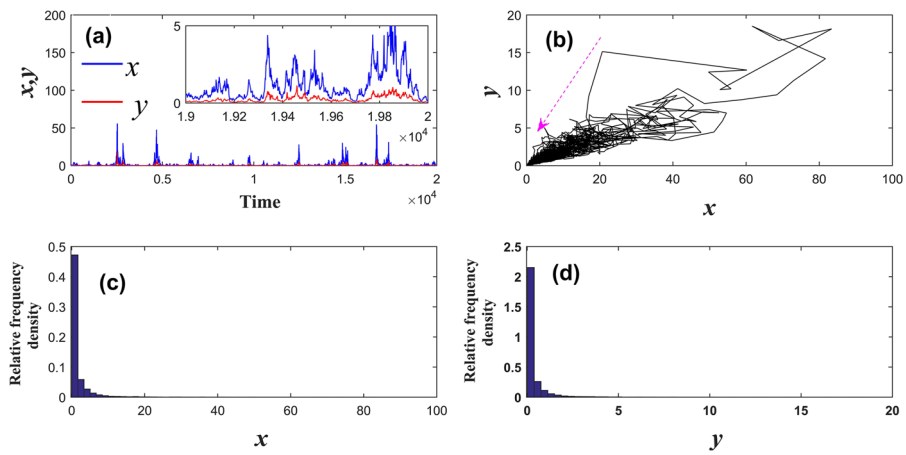

Fig. 6 **a** Time series diagram of System (2); **b** Phase trajectory of System (2) with the initial value $(4.5716, 0.9363)$ and the noise intensity $\sigma_1 = \sigma_2 = 0.5$; **c**, **d** show histograms of probability density function of x and y. Other parameter values are given in (3)

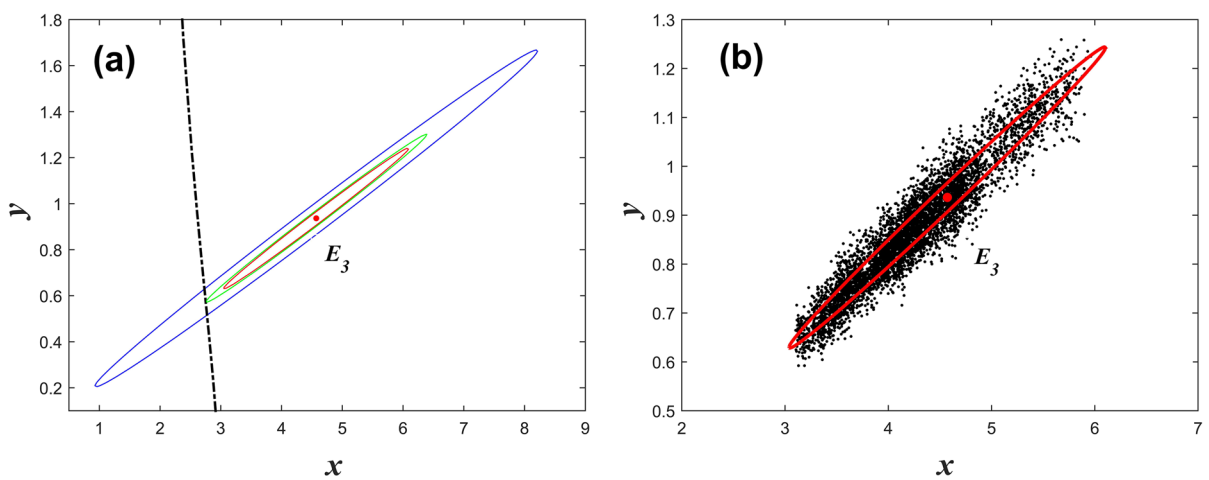

Fig. 7 **a** Separatrix (dashed-dotted) and confidence ellipses (solid) for $\sigma = 0.04$ (red),$\sigma = 0.0475$(green) and $\sigma = 0.095$ (blue); **b** Random states (black dots) of System (2) and confidence ellipse (red) for $\sigma = 0.04$. Other parameter values are given in (3). (Color figure online)

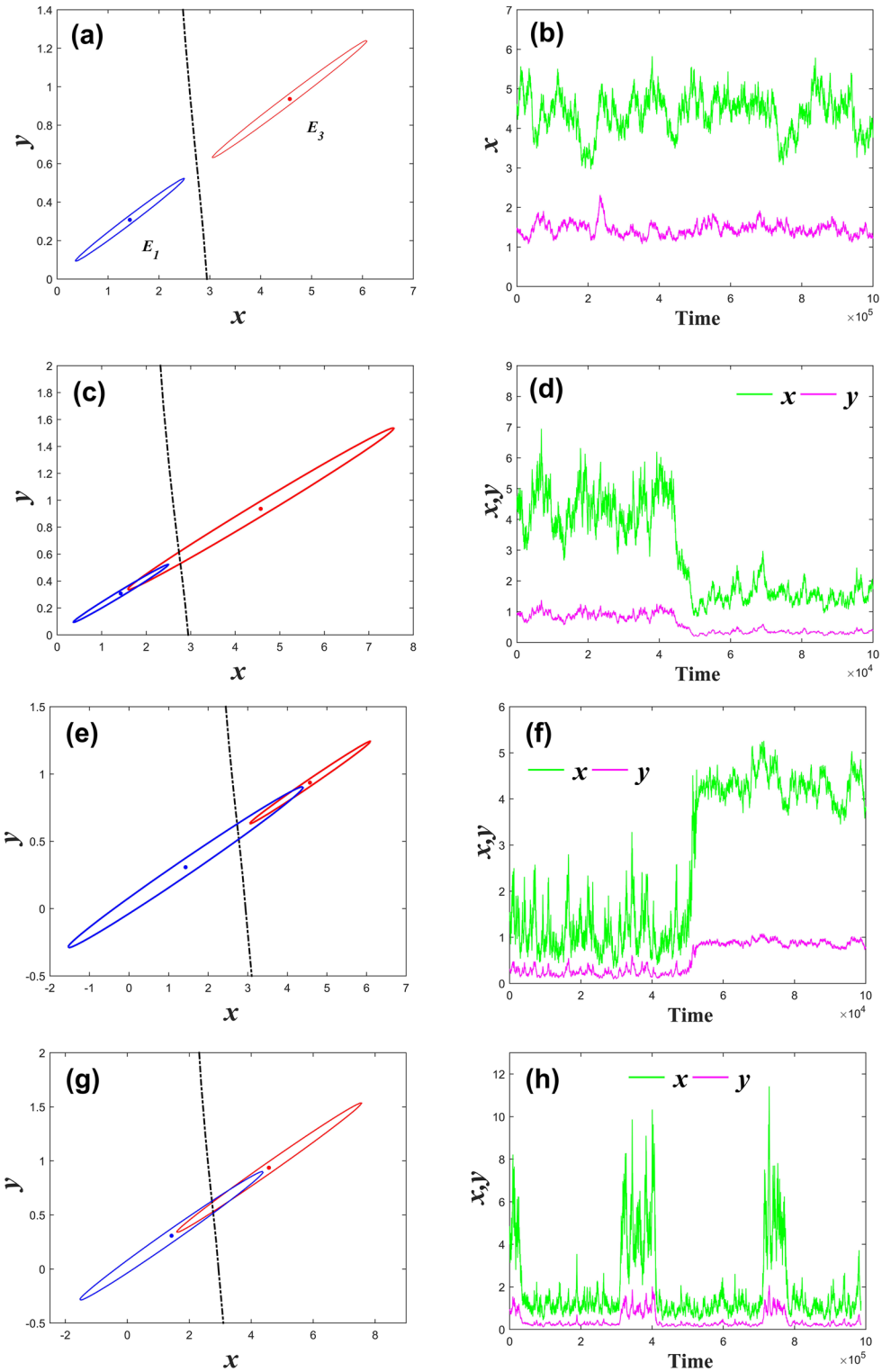

Fig. 8 The left subfigures represent the confidence ellipses, and the right subfigures represent the time series diagram of System (2). Here, $\sigma_1 = 0.101, \sigma_2 = 0.04$ in **a**, **b**; $\sigma_1 = 0.101, \sigma_2 = 0.078$ in **c**, **d**;$\sigma_1 = 0.278, \sigma_2 = 0.04$ in **e**, **f**;$\sigma_1 = 0.278, \sigma_2 = 0.078$ in **g**, **h**. Other parameter values are given in (3)

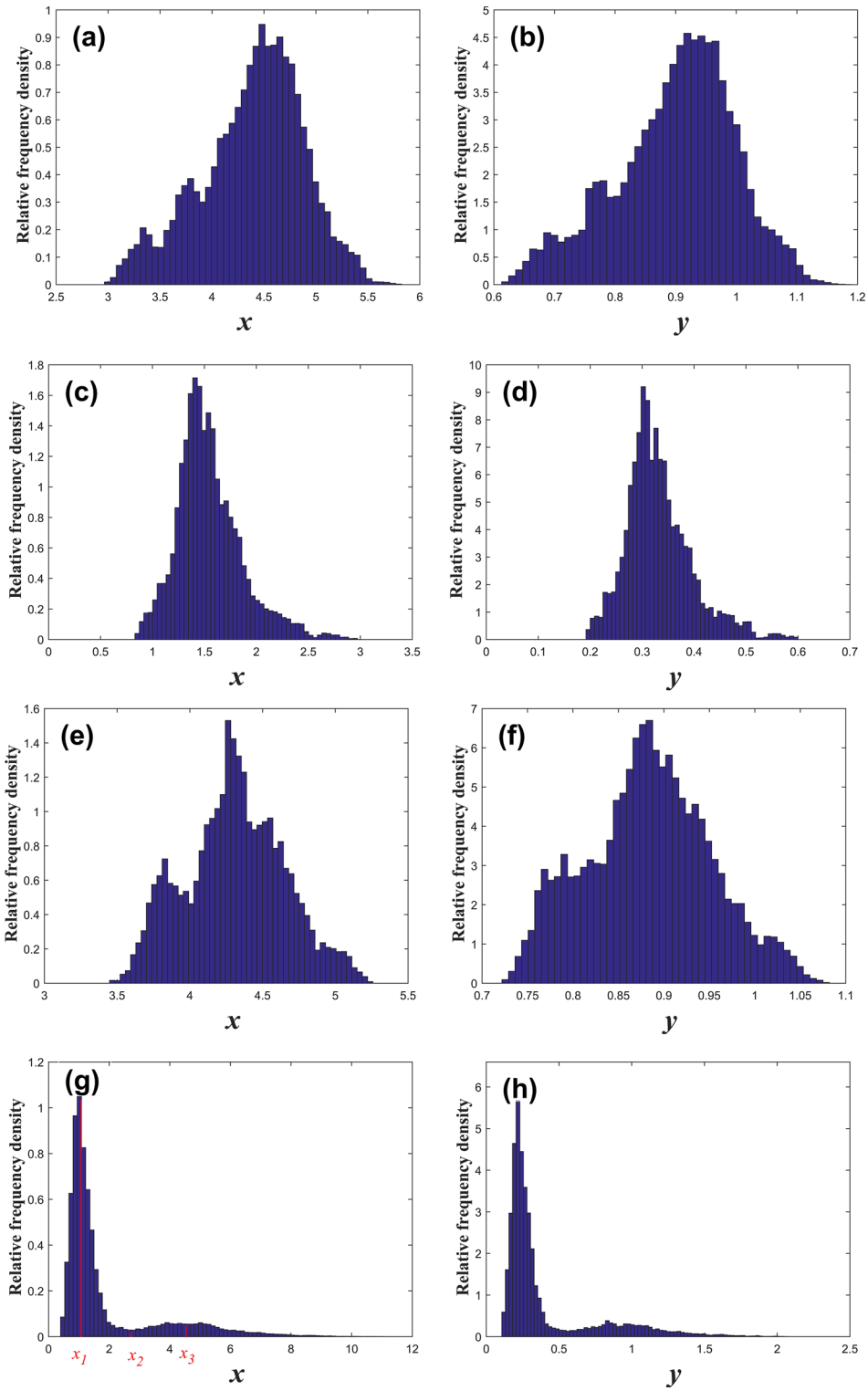

Fig. 9 **a**, **b** show histograms of probability density function of x and y in **b** of Fig. 8; **c**, **d** show histograms of probability density function of x and y in **d** of Fig. 8; **e**, **f** show histograms of probability density function of x and y in **f** of Fig. 8; **g**, **h** show histograms of probability density function of x and y in **h** of Fig. 8. Notice that this figure shows unimodal (monostabillity) for **a**–**f** and bimodal (bistable state) for **g**, **h**. Here, $x_i (i = 1, 2, 3)$ are the internal equilibria in **g**

To describe the configurational arrangement of the confidence ellipses of stochastic equilibria induced by noise, we let $\sigma = \sigma_1 = \sigma_2$ and take E_3 as an example in System (2). We fix $P = P_2 = 0.95$ and take three increasing noises $\sigma = 0.04$, 0.0475 and 0.095. Then configurational arrangements of the confidence ellipses at equilibrium E_3 are presented in Fig. 7a, which shows that as the noise intensity increases continuously, the confidence ellipse gradually expands and passes through the separatrix and eventually enters the attraction basin of coexistence equilibrium E_1. This implies that noise-induced tipping [31] occurs only when the confidence ellipse crosses the separatrix. When the confidence ellipse tangents to the separatrix, the noise intensity σ is defined as tipping threshold. In Fig. 7a, the tipping threshold is $\sigma^* \approx 0.0475$ (see green in Fig. 7a). When $\sigma > \sigma^*$, the trajectory of equilibrium E_3 leaves its attraction basin and finally stays near equilibrium E_1 with high probability. From Fig. 7b, we observe that the random states of System (2) are distributed around equilibrium E_3 with $\sigma = 0.04$, and they locate in the interior of confidence ellipse with probability 0.95. For equilibrium E_1, we have the similar results, which are not stated here.

Next, we consider how the two coexistence equilibria switch as σ_1 and σ_2 are not equal in (6) and (7). Let $P_1 = P_2 = 0.95$, we study the two confidence ellipses with σ_1 and σ_2. For weak noise, $\sigma_1 = 0.101, \sigma_2 = 0.04$, two confidence ellipses of two coexistence equilibria (E_1 and E_3) are obviously separated by the separatrix of attraction basins of these equilibria (see Fig. 8a), and the random solutions starting from one side of the separatrix finally stay near the equilibrium on this side (see Fig. 8b). It shows that weak noise induces the trajectories of $A\beta$ and Ca^{2+} to oscillate regularly and slightly near the coexistence equilibrium, which indicates that weak noise has a slight effect on the concentrations of $A\beta$ and Ca^{2+}. Fixing $\sigma_1 = 0.101$, as the noise intensity σ_2 increases to 0.078 and exceeds the tipping threshold ($\sigma_2^* = \sigma_*$), the confidence ellipse of equilibrium E_3 evidently crosses the separatrix (see Fig. 8c), and the random solutions starting from the attraction basin of equilibrium E_3 cross the separatrix and enter the attraction basin of equilibrium E_1(see Fig. 8d). For fixed $\sigma_2 = 0.04$, as the noise intensity σ_1 increases to 0.278, we can also get similar results (see Fig. 8e, f), which will not be stated here. More interestingly, we observe that when $\sigma_1 = 0.278, \sigma_2 = 0.078$, the confidence ellipses of two coexistence equilibria (E_1 and E_3) both cross the separatrix into each other's attraction basin and intersect each other (see Fig. 8g). The frequent jumps between two coexistence equilibria (E_1 and E_3) are also viewed (see Fig. 8h). The first three cases are associated with the initial value of the random trajectory (see Fig. 8b, d, f), while for the fourth case, the initial values can be chosen anywhere (see Fig. 8h). These findings provide a theoretical basis for the control of AD.

It is worthy to point out the phase transitions induced by noise are associated with shape changes of the probability density functions of $A\beta$ and Ca^{2+}. Notice that we take out the data of the stable random solution (after the first phase transition) in the time series diagrams in Fig. 8, and then draw Fig. 9. Taking E_3 as an example, when the noise intensity is less than σ_*, the probability density functions have a unique peak (see Figs. 8b, 9a, b). As noise intensity passes σ_*, the phase transition induced by noise occurs, noise-induced tipping occurs, which also shows a unique peak (see Figs. 8d, 9c, d). Similarly, at E_1, we can get the noise-induced phase transition as well (see Figs. 8f, 9e, f). As both σ_1 and σ_2 are greater than the tipping thresholds, System (2) exhibits two peaks at x_1, x_3, and a valley at x_2 ($x_1 < x_2 < x_3$) (see Figs. 8h, 9g, h), here, $x_i (i = 1, 2, 3)$ are the internal equilibria of System (1). This case shows multiple phase transitions, and represents a bimodal (located at x_1, x_3) reflected by probability density functions of x and y (see Fig. 9g, h). In a word, System (2) exhibits a monostable behavior for (a)–(f) in Fig. 9, and a bistable behavior for (g), (h) in Fig. 9. Therefore, the stationary density of System (2) undergoes the phase transitions from unimodal to bimodal distributions with both σ_1 and σ_2 increasing. However, such a phase transition is characteristic of stochastic system and does not exist in deterministic system.

In this subsection, we observe that three forms of phase transition are induced by noise: pathological state to healthy state switching (see Fig. 8d), healthy state to pathological state switching (see Fig. 8f) and the pathological state and healthy state switching many times in a long time (see Fig. 8g). In fact, it is possible to control the noise intensity by physical methods to alleviate AD. For example, physical

exercise therapy [35], repetitive transcranial magnetic stimulation [36] and positron emission tomography [40], in which physical methods have been used to treat AD, and the treatment has been very effective (e.g., improved cognitive ability). These treatment methods make the noise intensity reach the tipping threshold, which can also be said that the key point of the bistable switch toward the evolution of AD and can be used as an important indicator for the treatment of AD. So, it is possible to switch from pathological state to healthy state due to varying degrees of influence on noise intensity through treatment methods. Currently, there are no permanent drugs on the market to control AD, but controlling the noise intensity through physical methods may be a feasible strategy for the treatment of AD in future. Therefore, noise-induced phase transition may provide a theoretical basis for contemporary medicine to alleviate AD. It should be pointed out that the phenomenon of noise-induced phase transition has been found in many research fields and can explain some things that happen in ecosystems [29, 30, 47, 48] such as blooms in aquatic ecosystems [30], the two modes of survival of biological populations [48] and the species extinction [29].

Notice that Figs. 8 and 9 are based on the bistability of System (1). The two attractors (stable equilibria E_1, E_3) correspond to healthy and pathological equilibrium, respectively. Two attraction basins are distinctly separated by the separatrix, which is the stable manifold of saddle point E_2. Solutions from either side of separatrix will eventually approach the equilibrium (see Figs. 8a, b, 9a, b). However, when there is noise disturbance, the boundary may be damaged by noise, and the solutions in the attractive basin of one stable coexistence equilibrium can eventually approach the other stable coexistence equilibrium with a high probability (see Fig. 8c–h, 9c–h). That is, noise interference makes it possible to switch stability between random equilibria. Due to the inability to target the large area of neuron and synaptic death in AD brain, and the obstacles of drug transport across the impenetrable blood–brain barrier, as well as drug therapy is prone to side effects (see introduction), so drug therapy has reached the bottleneck at present. Thus controlling noise intensity with physical methods is likely to be the most promising treatment for AD in future.

4 Conclusion and discussion

At present, the modeling methods of AD models is very rare, most likely the pathogenesis of AD is accompanied by a highly complex ecological process. However, only a few models have been developed to elucidate specific and focal aspects for cerebral neurological disorders, such $A\beta$ aggregation [49], the APP kinetics [50] and the impact of the interaction between neurons, astrocyte and microglial cells on the formation of $A\beta$ [51]. It is well known that the stochastic variations from microenvironment inside the cell cannot be ignored, but there are very few achievements on how the stochastic variations in the microenvironment of $A\beta$ and Ca^{2+} affect the development of AD. In this paper, we introduced extrinsic noise into the deterministic system to study how extrinsic noise affects the development of AD. Here, we mainly studied, on the one hand, the impacts of positive feedback and periodic treatment on AD in the deterministic system; on the other hand, the global and ergodic properties of stochastic solutions and noise-induced phase transitions. Our results can qualitatively explain the dynamic process that triggers AD and the noise-induced phase transition may become one of the effective means to treat AD.

For the deterministic system (1), we discussed the impacts of the positive feedback strength (reflected by V_3) between $A\beta$ and Ca^{2+} on the development of AD. With the increase of V_3, System (1) can undergo saddle-node bifurcations. For certain range of V_3, System (1) exhibits a node–node bistability (two stable equilibria coexist). Since the dynamics is initial condition dependent, we can adjust the initial concentrations of $A\beta$ and Ca^{2+} to mitigate the development of AD. However, as the positive feedback strength exceeds the threshold (V_3^{**}), the concentrations of $A\beta$ and Ca^{2+} are always in a pathological state. Moreover, we proposed two periodic treatment feasible drug strategies to alleviate AD and screened out more effective one. This also demonstrates that periodic drug treatment can keep concentrations of $A\beta$ and Ca^{2+} in the attraction basin in healthy state, even the positive feedback strength exceeds the threshold (reflected by V_3) (see Figs. 1, 2), and it also indirectly reflects that following the doctor's advice and taking drugs scientifically play an important role in the recovery of the patients. For the stochastic system (2),

we analyzed the existence and uniqueness of global positive solutions and established sufficient conditions for the existence of ergodic stationary distribution. We also constructed confidence ellipses to study the noise-induced switch between two random coexistence equilibria and estimated the tipping threshold. Our results showed that the change of noise intensity can lead to stochastic switching between pathological and healthy state. Our results may provide new ideas for the medical field to alleviate AD.

Clinical diagnosis has shown that the patients with AD have a significant reduction in the acetylcholine neurotransmitter in their brain [52]. Some acetylcholinesterase inhibitors on the market [3, 53, 54] can enhance acetylcholine system by inhibiting acetylcholinesterase and $A\beta$-targeting clearance [3, 55]. Moreover, repetitive transcranial magnetic stimulation and positron emission tomography in physical therapy are used as a noninvasive treatment for neurological diseases, and currently physical therapy has shown significant reductions in the concentration of $A\beta$ and also improved the patient's cognitive ability [36, 40]. It should be noted that the National Institute on Aging and the Alzheimer's Association suggested that level of $A\beta$ is an important indicator of detecting AD [56, 57], and some biomarker tests to detect the level of $A\beta$ have been used as an auxiliary method to diagnose AD, including beta-amyloid PET imaging, cerebrospinal fluid testing, features of the superficial white matter and impaired LTP-like cortical plasticity [36, 58–60]. In addition, gene therapy, $A\beta$ immunotherapy and nanotechnology can also alleviate the development of AD [3, 37, 61]. Therefore, we concluded that we can control the noise intensity through physical therapy to make System undergo phase transition (see Figs. 8, 9), which makes it possible to achieve low concentration of $A\beta$. This also provides theoretical support for the control of AD in the medical field. We expect that noise-induced phase change provides a possibility to cure AD completely in future.

In this paper, we studied the effect of two periodic feasible drug strategies on the progression of AD, and presented the basic results of stochastic system including the uniqueness and existence and ergodic stationary distribution of solution. We also investigated noise-induced switching between stable equilibria, which suggests that noise may induce reduction in the $A\beta$ concentration. Therefore, we can view the random disturbance in System as a control variable, such as language training and physical therapy, to achieve the control of AD, thereby slowing the deterioration of AD. The introduction of the Brownian motion in System (2) has been proven to be a useful technique to capture molecular trails in experimental settings. Therefore, our numerical analysis can provide real-time observation of the concentration of $A\beta$ in different time periods. This mathematical approach can be a promising quantitative screening device for AD therapy, especially in the context of early diagnosis and disease evolution predictions.

However, we here studied just the most basic dynamics of $A\beta$ and Ca^{2+}, but there is a need for further research on the mechanism of AD. For example, silibinin, a flavonoid compound, selectively interacts with $A\beta$ monomer to reduce its aggregation and alleviate neuronal damage. Spread of misfolded proteins by "prion-like" protein aggregation, and soluble oligomers bind with high affinity to prion proteins, which is mediated by the protein and produces toxic damage neurons on the surface of the cell [39]. Thus, the interaction between these molecules affects the development of AD. In addition, some substances in the brain have diffusion behavior, e. g., Achdou et al. [62] proposed a mathematical model at the early stage of AD based on aggregation equation to account for the diffusion. Therefore, spatial diffusion has a certain influence on the development of AD. And the effect of intrinsic noise on $A\beta$ and Ca^{2+} metabolism is often ignored, it will be interesting to combine intrinsic noises with extrinsic noises and discuss their joint influence on the dynamics of AD system. We regard these studies as our future work.

Acknowledgments We are grateful to two anonymous reviewers and the editor for their helpful comments.

Funding This work was supported by NSERC Individual Discovery Grant (No. RGPIN-2020-03911), NSERC Discovery Accelerator Supplement Award (No. RGPAS-2020-00090), NSFC-Yunnan United fund (No. U2102221). JZG is partially supported by a CSC Doctoral Scholarship.

Data availability The manuscript has no associated data.

Declarations

Conflict of interest All the authors declare that they have no conflict of interest.

Appendix

From the second equation of the deterministic system (i.e., $\sigma_1 = \sigma_2 = 0$ in (2)), we have

$$y = \frac{V_4 x + V_2}{k_2}. \tag{A.1}$$

The bring (A.1) into the first equation of the deterministic system, we get a cubic equation in one variable with respect to x

$$F(x) = T_3 x^3 + T_2 x^2 + T_1 x + T_0 = 0, \tag{A.2}$$

where

$$\begin{aligned}
T_3 &= -k_1 V_4^2, \\
T_2 &= -2V_2 V_4 k_1 + V_4^2 (V_1 + V_3), \\
T_1 &= 2V_2 V_4 (V_1 + V_3) - \left(V_2^2 + k_2^2 k_3^2\right) k_1, \\
T_0 &= V_2^2 (V_1 + V_3) + V_1 k_2^2 k_3^2.
\end{aligned}$$

We assume that (A.2) has three positive equilibria, x_1, x_2 and x_3 ($x_1 < x_2 < x_3$). $F'(x_1)$ is the derivative of $F(x)$ at x_i. We can easily get that $F'(x_1) < 0$, $F'(x_2) > 0$ and $F'(x_3) < 0$. Next, we give the stability analysis of the equilibria.

Calculate the Jacobian matrix $J(E_i)$ of the deterministic system at internal equilibrium $E_i(x_i, y_i)$

$$J(E_i) = \begin{pmatrix} -k_1 & \dfrac{2V_3 k_3^2 y_i}{\left(k_3^2 + y_i^2\right)^2} \\ \dfrac{V_4}{\varepsilon} & -\dfrac{k_2}{\varepsilon} \end{pmatrix}.$$

The eigenvalues of $J(E_i)$ satisfy the equation:

$$\lambda^2 - \mathrm{tr}(J)\lambda + \mathrm{Det}(J) = 0,$$

where,

$$\mathrm{tr}(J) = -k_1 - \frac{k_2}{\varepsilon} < 0, \quad \mathrm{Det}(J) = -\frac{(V_4 x_i + V_2) F'(x_i)}{k_2 y_i \left(k_3^2 + y_i^2\right)},$$

because $F'(x_1) < 0$, $F'(x_2) > 0$ and $F'(x_3) < 0$, so E_1 and E_3 are asymptotically stable and E_2 is an unstable saddle point.

In addition, the two equations on the right of the deterministic system are respectively defined as H_1 and H_2, then

$$\frac{\partial H_1}{\partial x} + \frac{\partial H_2}{\partial y} = -k_1 - \frac{k_2}{\varepsilon} < 0.$$

According to the Bendixson–Dulac criteria, it is clear that there is no closed orbit in the deterministic system, that is, when the deterministic system has a unique equilibrium, it must be globally asymptotically stable.

References

1. Caluwé, D.J., Dupont, G.: The progression towards Alzheimer's disease described as a bistable switch arising from the positive loop between amyloids and Ca^{2+}. J. Theor. Biol. **331**, 12–18 (2013)
2. William, A., Markesbery, R.: Oxidative stress hypothesis in alzheimer's disease. Free Radic. Biol. Med. **23**(1), 134–147 (1997)
3. Ewen, S.T., Fauzi, A., Quan, T.Y., Chamyuang, S., Yin, A.: A review on advances of treatment modalities for Alzheimer's disease. Life Sci. **276**, 119129 (2021)
4. Reisberg, B., Ferris, S.H., De, L.M.J., Crook, T.: The global deterioration scale for assessment of primary degenerative dementia. Am. J. Psychiatry **139**(9), 1136–1139 (1982)
5. Kang, Y.J., Diep, Y.N., Tran, M., Cho, H.: Therapeutic targeting strategies for early-to late-staged alzheimer's disease. Int. J. Mol. Sci. **21**(24), 1–34 (2020)
6. Zanetti, O., Solerte, S.B., Cantoni, F.: Life expectancy in Alzheimer's disease (AD). Arch. Gerontol. Geriatr. **49**, 237–243 (2009)
7. Hirtz, D.G., Thurman, D.J., Gwinn-Hardy, K., Mohamed, M., Zalutsky, R.: How common are the "common" neurologic disorders? Neurology **68**(5), 326–337 (2007)
8. Wimo, A., Guerchet, M., Ali, G.C., Wu, Y.T., Matthew, A.: The worldwide costs of dementia 2015 and comparisons with 2010. Alzheimer's Dement. **13**(1), 1–7 (2017)
9. Hu, J., Zhang, Q., Meyer-Aese, A., Ye, M.: Stationary distribution of a stochastic Alzheimer's disease model. Math. Method. Appl. Sci. **43**(17), 1–13 (2020)
10. Sweeney, M.D., Kisler, K., Montagne, A., Toga, A.W., Zlokovic, B.V.: The role of brain vasculature in neurodegenerative disorders. Nat. Neurosci. **13**, 18–31 (2018)
11. Ma, J.: Biophysical neurons, energy, and synapse controllability: a review. J. Zhejiang Univ. Sci. A **24**(2), 109–129 (2023)
12. Li, H.X., Zhao, H.Y.: Mathematical model of Alzheimer's disease with prion proteins interactions and treatment. Appl. Math. Comput. **433**(15), 127377 (2022)
13. Dayeh, M.A., Livadiotis, G., Elaydi, S.: A discrete mathematical model for the aggregation of β-amyloid. PLoS ONE **13**(5), e0196402 (2018)
14. Hu, J., Zhang, Q.M., Meyer-Baese, A., Ye, M.: Stability in distribution for a stochastic Alzheimer's disease model with reaction diffusion. Nonlinear Dyn. **108**, 4243–4260 (2022)
15. Helal, M., Hingant, E., Pujo-Menjouet, L., Webb, G.F.: Alzheimer's disease: analysis of a mathematical model incorporating the role of prions. J. Math. Biol. **69**(5), 1207–1235 (2014)

16. Hao, W., Friedman, A.: Mathematical model on Alzheimer's disease. BMC Syst. Biol. **10**(1), 108 (2016)
17. Asili, E., Yarahmadian, S., Khani, H., Sharify, M.: A mathematical model for amyloid-β aggregation in the presence of metal ions: a timescale analysis for the progress of alzheimer disease. Bull. Math. Biol. **81**(6), 108 (2019)
18. Angelo, D., Erene, M., Kayed, R., Milton, S.C., Ian, P., Charles, G.G.: Calcium dysregulation and membrane disruption as a ubiquitous neurotoxic mechanism of soluble amyloid oligomers. J. Biol. Chem. **280**(17), 17294–17300 (2005)
19. Kuchibhotla, K.V., Goldman, S.T., Lattarulo, C.R., Wu, H.Y., Hyman, B.T., Bacskai, B.J.: Aβ plaques lead to aberrant regulation of calcium homeostasis in vivo resulting in structural and functional disruption of neuronal networks. Neuron **59**(2), 214–225 (2008)
20. Berridge, M.: Calcium signalling and Alzheimer's disease. Neurochem. Res. **36**(7), 1149–1156 (2011)
21. Ho, M., Hoke, D.E., Chua, Y.J., Li, Q.X., Culvenor, J.G., Masters, C., et al.: Effect of metal chelators on r-secretsindicates that calcium and magnesium ions facilitate cleavage of Alzheimer amyloid precursor substrate. Int. J. Alzheimers Dis. **2011**(6106), 950932 (2010)
22. Dighe, S.N., Mora, E., Chan, S., Kantham, S., Ross, B.P.: Rivastigmine and metabolite analogues with putative Alzheimer's disease-modifying properties in a caenorhabditis elegans model. Commun. Chem. **2**(1), 1–13 (2019)
23. Pierrot, N., Ghisdal, P., Caumont, A., Jean, N.O.: Intraneuronal amyloid-β1-42 production triggered by sustained increase of cytosolic calcium concentration induces neuronal death. J. Neurochem. **88**(5), 1140–1150 (2004)
24. Eugene, S., Xue, W.F., Robert, P., Doumic, M.: Insights into the variability of nucleated amyloid polymerization by a minimalistic model of stochastic protein assembly. J. Chem. Phys. **144**(17), 175101 (2016)
25. Theriault, P., Elali, A., Rivest, S.: The dynamics of monocytes and microglia in Alzheimer's disease. Alzheimers Res. Ther. **7**(1), 1–10 (2015)
26. Falcke, M.: Reading the patterns in living cells-the physics of Ca^{2+} signaling. Adv. Phys. **53**(3), 255–440 (2004)
27. Bashkirtseva, I., Ryazanova, T., Ryashko, L.: Confidence domains in the analysis of noise-induced transition to chaos for goodwin model of business cycles. Int. J. Bifurc. Chaos **24**(8), 1–10 (2014)
28. Xu, C.Q., Yuan, S.L., Zhang, T.H.: Stochastic sensitivity analysis for a competitive turbidostat model with inhibitory nutrients. Int. J. Bifurc. Chaos **26**(10), 1650173 (2016)
29. Xu, C.Q., Yuan, S.L., Zhang, T.H.: Sensitivity analysis and feedback control of noise-induced extinction for competition chemostat model with mutualism. Phys. A **505**, 891–902 (2018)
30. Zhao, S.N., Yuan, S.L., Zhang, T.H.: The impact of environmental fluctuations on a plankton model with toxin-producing phytoplankton and patchy agglomeration. Chaos Solitons Fractal **162**, 112426 (2020)
31. Alkhayuon, H., Tyson, R.C., Wieczorek, S.: Phase-sensitive tipping: how cyclic ecosystems respond to contemporary climate. Proc. R. Soc. A **477**, 20210059 (2021)
32. Mattson, M.P., Bezprozvanny, I.: Neuronal calcium mishandling and the pathogenesis of Alzheimer's disease. Trends Neurosci. **31**(9), 454–463 (2008)
33. Bojarski, L., Herms, J., Kuznicki, J.: Calcium dysregulation in Alzheimer's disease. Neurochem. Int. **52**(4), 621–633 (2008)
34. Berridge, M.: Calcium hypothesis of Alzheimer's disease. Eur. J. Physiol. **459**(3), 441–449 (2010)
35. Rosa, A., Olaso-Gonzalez, G., Arc-Chagnaud, C., Millan, F., Salvador-Pascual, A.: Physical exercise in the prevention and treatment of Alzheimer's disease. J. Sport Health Sci. **9**(5), 394–404 (2020)
36. Li, X.X., Qi, G.Q., Yu, C., Lian, G.M., Zheng, H., Wu, S.C., et al.: Cortical plasticity is correlated with cognitive improvement in Alzheimer's disease patients after rTMS treatment. Brain Stimul. **14**(3), 503–510 (2021)
37. Tatiaparti, K., Sau, S., Rauf, M.A., Iyer, A.K.: Smart treatment strategies for alleviating tauopathy and neuroinflammation to improve clinical outcome in Alzheimer's disease. Drug Discov. Today **25**(12), 2110–2129 (2020)
38. Wang, Y.H., Xu, X.Y., Zhu, Y.T., Wang, R.B.: Neural energy mechanism and neurodynamics of memory transformation. Nonlinear Dyn. **97**(1), 697–714 (2019)
39. Sun, X.J., Si, H.: Population rate coding in recurrent neuronal networks consisting of neurons with mixed excitatory–inhibitory synapses. Nonlinear Dyn. **100**, 2673–2686 (2020)
40. Fleming, V., Piro-Gambetti, B., Patrick, A., Zammi, M., Alexander, A.: Physical activity and cognitive and imaging biomarkers of Alzheimer's disease in down syndrome. Neurobiol. Aging **107**, 118–127 (2021)
41. Higham, D.J.: An algorithmic introduction to numerical simulation of stochastic differential equations. SIAM Rev. **43**(3), 525–546 (2001)
42. Mao, X.: Stochastic Differential Equations and Applications, 2nd edn. Woodhead, Cambridge (2008)
43. Hasminskii, R.Z.: Stochastic Stability of Differential Equations. Springer, Berlin (1980)
44. Gard, T.: Introduction to Stochastic Differential Equations. Marcel Dekker Inc., New York (1988)
45. Strang, G.: Linear Algebra and Its Applications. Thomson Learning Inc., Chicago (1988)
46. Zhu, C., Yin, G.: Asymptotic properties of hybrid diffusion systems. SIAM J. Control Optim. **46**, 1155–1179 (2007)
47. Yuan, S., Wu, D., Lan, G., Wang, H.: Noise-induced transitions in a nonsmooth producer–grazer model with stoichiometric constraints. Bull. Math. Biol. **82**(5), 55 (2020)
48. Zhang, S.Q., Yuan, S.L., Zhang, T.H.: A predator-prey model with different response functions to juvenile and adult prey in deterministic and stochastic environments. Appl. Math. Comput. **413**, 126598 (2022)
49. Pallitto, M., Murphy, R.: A mathematical model of the kinetics of β-amyloid fibril growth from the denaturated state. Biophys. J. **81**(3), 1805–1822 (2001)
50. Ortega, F., Stott, J., Visser, S., Bendtsen, C.: Interplay between α, β, and γ-secretases determines biphasic amyloid-β level in the presence of γ-secretases inhibitor. J. Biol. Chem. **288**(2), 785–792 (2013)
51. Puri, I., Li, L.: Mathematical modeling for the pathogenesis of Alzheimer's disease. PLoS ONE **5**(12), e15176 (2010)
52. Murray, A., Faraoni, M., Castro, M., Alza, N., Cavallaro, V.: Natural AChE inhibitors from plants and their contribution to Alzheimer's disease therapy. Curr. Neuropharmacol. **11**(4), 388–413 (2013)

53. Rashid, T., Mithila, D., Safin, A., Ajit, G.: Advances on plant extracts and phytocompounds with acetylcholinesterase inhibition activity for possible treatment of Alzheimer's disease. Phytomedicine Plus **2**(1), 100184 (2021)
54. Srivastava, S., Ahmad, R., Khare, S.K.: Alzheimer's disease and its treatment by different approaches: a review. Eur. J. Med. Chem. **216**, 113320 (2021)
55. Zhang, H.Q., Zhao, Y.P., Yu, M., Zhao, Z.Q., Liu, P.X., Cheng, H., et al.: Reassembly of native components with donepezil to execute dual-missions in Alzheimer's disease therapy. J. Control. Release **296**, 14–28 (2019)
56. Assoc, A.: Alzheimer's disease facts and figures. Alzheimers Dement. **14**(3), 367–429 (2018)
57. Sperling, R.A., Aisen, P.S., Beckett, L.A.: Toward defining the preclinical stages of Alzheimer's disease: recommendations from the national institute on aging-Alzheimer's association workgroups on diagnostic guidelines for Alzheimer's disease. Alzheimers Dement. **7**(3), 280–292 (2011)
58. Forsberg, A., Engler, H., Almkvist, O.: PET imaging of amyloid deposition in patients with mild cognitive impairment. Neurobiol. Aging **29**(10), 1456–1465 (2008)
59. Palmqvist, S., Zetterberg, H., Mattsson, N.: Detailed comparison of amyloid PET and CSF biomarkers for identifying early Alzheimer disease. Neurology **85**(14), 1240–1249 (2015)
60. Bigham, B., Zamanpour, S.A., Zare, H.: Features of the superficial white matter as biomarkers for the detection of Alzheimer's disease and mild cognitive impairment: a diffusion tensor imaging study. Heliyon **8**(1), e08725 (2022)
61. Owens, L.V., Benedetto, A., Dawson, N., Gaffney, C.J., Parkin, E.T.: Gene therapy-mediated enhancement of protective protein expression for the treatment of Alzheimer's disease. Brain Res. **1753**, 147264 (2021)
62. Achdou, Y., Franchi, B., Marcello, N., Tesi, M.C.: A qualitative model for aggregation and diffusion of β-amyloid in Alzheimer's disease. J. Math. Biol. **67**(6), 1369–1392 (2013)